VOL.39 Nº1 2022
https://doi.org/10.22491/IMECTA.10844.en

Behavior to a cyclic fracture of an ASTM 316 stainless steel

Pedro G S Passalini*[a], Ricardo P Weber[a], Paulo F S Filho[b]
[a]Instituto Militar de Engenharia (IME)
Praça General Tibúrcio, 80, 22290-270, Praia Vermelha, Rio de Janeiro, RJ, Brazil.
[b]Instituto Federal do Rio de Janeiro (IFRJ), Mechanical Engineering Department, Paracambi, Rio de Janeiro.
***pedroguilhermesp2@hotmail.com**

ABSTRACT: The study of the fractography of a material is essential because it enables to reach the reason and conditions by which a material may break. Austenitic stainless steels show a macroscope aspect of ductile fracture when subjected to uniaxial loadings, with low rates of deformation until rupture. However, a detailed analysis by techniques, such as scanning electron microscopy (SEM), may show fragile fracture regions, which can occur due to the phase transformation that austenitic steels show when subjected to plastic deformation (TRIP effect) or hardened austenite. This study aims to evaluate the fracture aspect of a 316 stainless steel subjected to low frequency uniaxial cyclic loading to compare with the fracture aspect of the same fractured material in a tensile test, verifying how the change in the type of loading can affect the material's fracture morphology. The results indicate that both types of loading show a ductile fracture, but with different morphologies, that is, cup and cone type for tensile, and rupture at 45° for cyclic test. This difference indicates that the crack nucleates in different regions for each loading and may depend on the amount of material that is hardened and transformed during each test.

KEYWORDS: Fractography. ASTM 316 stainless steel. Cyclic test. Tensile Test.

RESUMO: O estudo da fractografia de um material é de extrema importância, pois, através do mesmo, é possível chegar a conclusões que indicam o motivo e as condições pelas quais um material pode vir a romper-se. Aços inoxidáveis austeníticos, quando submetidos a carregamentos uniaxiais, com baixas taxas de deformação até a ruptura, apresentam um aspecto macroscópio de fratura dúctil, entretanto, uma análise detalhada por técnicas, como microscopia eletrônica de varredura (MEV), podem mostrar regiões de fratura frágil, o que pode ocorrer pela transformação de fase que os aços austeníticos apresentam quando submetidos à deformação plástica (efeito TRIP) ou pela austenita encruada. Este trabalho tem como objetivo avaliar o aspecto de fratura de um aço inoxidável 316, submetido a carregamento cíclico uniaxial de baixa frequência para fins comparativos, com o aspecto de fratura do mesmo material fraturado em um ensaio de tração, verificando como a mudança do tipo de carregamento pode afetar na morfologia de fratura do material. Os resultados indicam que ambos os tipos de carregamento apresentam fratura dúctil, porém com morfologias diferentes, ou seja, tipo taça e cone para tração, e ruptura em 45° para o ensaio cíclico. Essa diferença indica que a trinca se nucleia em diferentes regiões para cada carregamento, podendo também indicar serem dependentes da quantidade de material encruado e transformado durante cada ensaio.

PALAVRAS-CHAVE: Fractografia. Aço inoxidável ASTM 316. Ensaio cíclico. Ensaio de Tração.

1. Introduction

ASTM 316 stainless steel is essential to the industry due to its corrosion resistance [1][2] and ductility [3]. Many sectors use it, such as the petrochemicals, food, pharmaceutical equipment, water transport, armament, among others [4][5].

The 316 stainless steel has an austenitic microstructure [6], which, since it is metastable [7], tends to microstructurally change when subjected to plastic deformation, that is, transforming its austenitic microstructure into martensitic, more fragile. This process is the TRIP effect (plasticity induced by phase transformation), which was first observed around 1950 [8][9].

Many studies indicate that the TRIP effect is able to significantly reduce the cracks produced by fatigue in steel with austenitic microstructure [7][10][11][12], probably due to the microstructural change during its deformation, which indicates the greater the deformation in the material the greater effect [13].

Li et al., 2021 [14] performed monotonous tensile tests on a 308L stainless steel. By macroscopically and microscopically analyzing the aspect of the fracture of the material, the authors concluded that it was ruptured by a ductile fracture. The scanning electron

microscopy (SEM) showed voids ("dimples") on the fracture surface of the specimen, indicating a ductile fracture of the material.

Lall et al., 2021 [15] observed fibrous regions with abundant presence of voids, typical of a ductile fracture, in the center of the fracture surface of an ASTM 709 austenitic stainless steel subjected to a tensile test, and cleavage regions at the edges of the surface, which characterizes a fragile fracture region [15].

Alsmadi et al., 2020 [16] performed low uniaxial cycle tests and high deformation amplitudes in a 709 austenitic steel. They observed three regions: the first was identified as the nucleation point of the crack, the second as striation regions, that is, of propagation of cracks, and the third as overload regions with a ductile aspect, indicated by the presence of voids [16].

This study aimed to evaluate and compare the fracture aspect of ASTM 316 austenitic stainless steel, monotonically tensile-tested and cyclic-tested, to verify if there was fractographic change according to the type of loading employed.

2. Materials and methods

The material used in this study was ASTM 316 stainless steel. Its chemical composition is described in **Table 1**. Specimens (S) were produced according to the norm E606-92/12 [17] for uniaxial and cyclic tests. The S dimensions are shown in **Figure 1**.

Tab. 1 – Chemical composition of the ASTM 316 stainless steel.

Ele.	C	Si	Mn	P	S
%p	0.018	0.33	1.44	0.035	0.025
Ele.	Co	Cr	Ni	Cu	N
%p	0.09	17.0	10.16	0.25	0.064

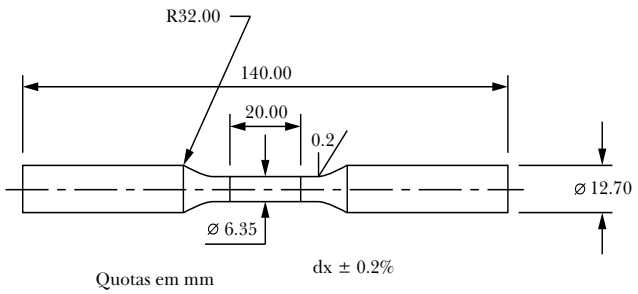

Fig. 1 – S dimensions. Source: [17].

The tensile and cyclic tests were performed in a servo-hydraulic machine, Shimadzu Servopulser model (**Figure 2**), with a 5 Mpa pressure in the claws. A Dynastrain extensometer was used in the tensile test. The cyclic test was controlled by the maximum and minimum forces of 14kN and -14kN (traction × compression), thus varying the deformation at a frequency of 0.075Hz until rupture.

Fig. 2 – Universal test machine used in this study.

The analyses of the fracture aspects for both tests were performed by the scanning electron microscopy (SEM) technique. Using secondary electrons detector at an acceleration voltage of 10.00kV and spot size of 5.0.

3. Results and discussion

3.1 Tensile test

Figure 3 shows the curve obtained by the tensile test. The result expresses the typical behavior of a ductile material [18].

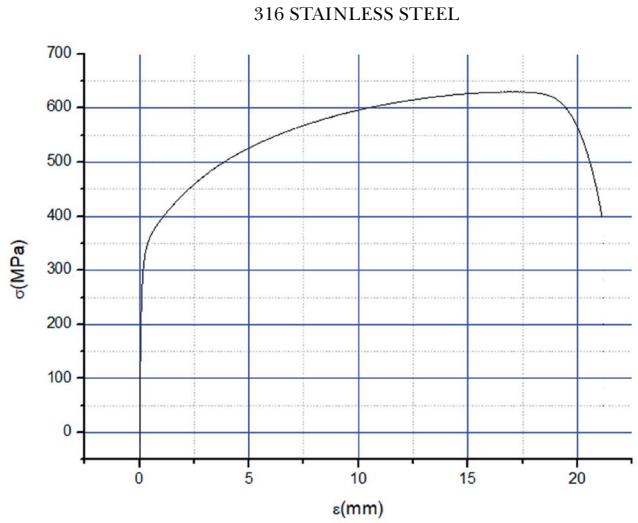

Fig. 3 – Stress × strain curve for a tensile-tested material.

Figure 4 shows the fracture for the tensile test in which we verified a cup and cone morphology, typical of the ductile fracture [19], with cleavage regions at the edges, which shows that the nucleation of the crack came from the center of the S [20]. In a closer analysis (**Figure 5**), we identified dimples, which indicate regions of ductile fracture, and cleavage points, which indicate fragile fracture [21]. These points may have been formed by the hardened austenite or by a fraction of the material transformed by the TRIP effect [22].

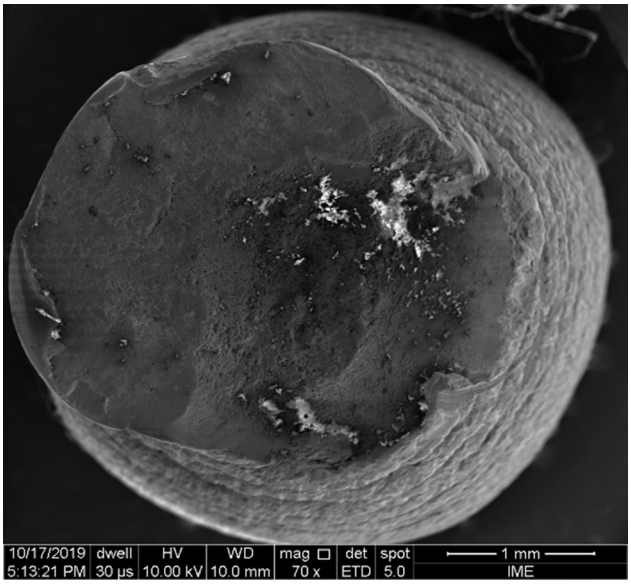

Fig. 4 – Micrograph obtained by SEM for steel fracture in a tensile-tested study.

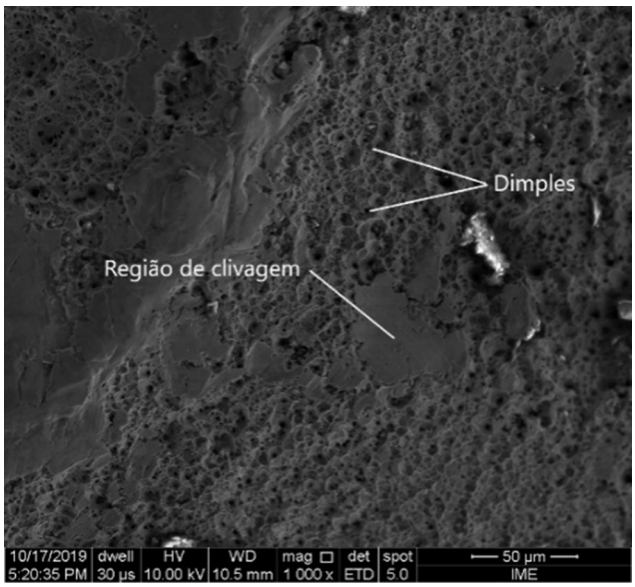

Fig. 5 – Close micrograph obtained by SEM for the fracture of steel in a tensile-tested study.

3.2 Cyclic test

Figure 6 shows the characteristic curve obtained in the cyclic test. We performed the cyclic loading at a stress above the flow stress of the material, which caused it to break with 220 cycles.

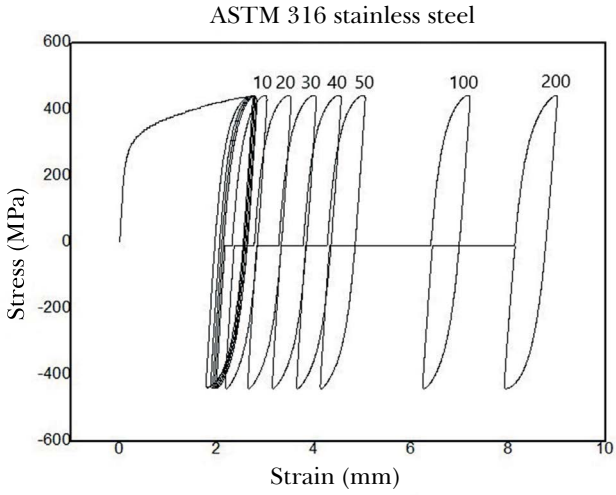

Fig. 6 – Stress × strain curve for the cyclic-tested material (its number is indicated above each formed cycle).

Three regions (1,2,3) with shear fracture aspect show an inclination of 45° (**Figure 7**) on the fracture surface of the cyclic-tested material [23]. A close image (**Figure 8**) of these regions indicates the presence of voids [24].

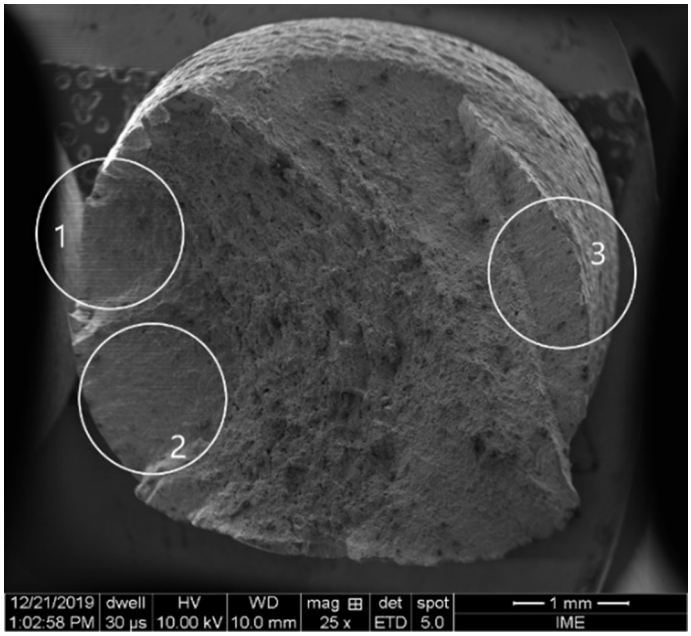

Fig. 7 – Micrograph obtained by SEM for steel fracture in a cyclic-tested study.

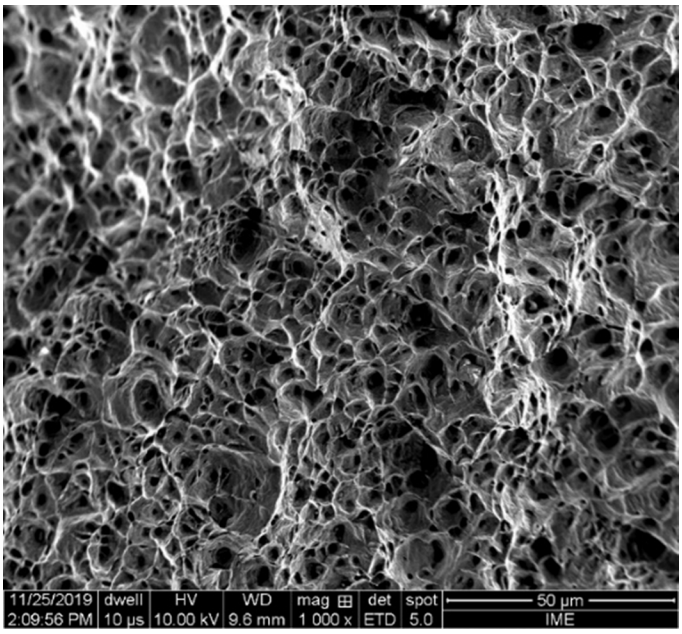

Fig. 8 – Close micrograph obtained by SEM for steel fracture in a cyclic-tested study.

4. Conclusion

We concluded that the microscopic aspects for both tests were of a ductile fracture, but differed in their morphology, being cup and cone type for tensile, and rupture in 45° for the cyclic test. This difference indicates that the crack nucleates in different regions for each type of loading and may depend on the amount of material hardened and transformed during each test, which directly influences how the cracks will propagate.

Acknowledgements

The authors thank the IME and UFF for the structure provided and CAPES for their financial support.

References

[1] ABBAS, A. T.; ANWAR, S.; ABDELNASSER, E.; LUGMAN, M.; QUDEIRI, J. E. A.; ELKASEER, A. Effect of diferente coocling strategies on surface quality and power consumption in finishing end milling of stainless steel 316; **Materials**, 14, 903, 2021.

[2] HOPPIUS, J. S.; KUKREJA, L. M.; KNYAZEVA, M.; PÖHL, F.; WALTHER, F.; OSTENDORF, A.; GUREVICH, E. L. On femtosecond laser shock peening of stainless steel AISI 316; **Applied Surface Science**, 435,, 2018, pp.1120-1124.

[3] XIONG, Y.; YUE, Y.; LU, Y.; HE, T.; FAN, M.; REN, F.; CAO, W. Cryorolling impacts on microstructure and mechanical properties of AISI 316 LN austenitic stainless steel; **Materials Science & Engineering**: A., 709, 2018, pp. 270-276.

[4] WILLIAMS, D. F.; KELLAR, E. J. C.; JESSON, D. A.; WATTS, J. F. Surface analysis of 316 stainless steel teated with cold atmospheric plasma; **Applied Surface Science**, 403, 2018, pp. 240-247.

[5] HUTLI, E.; NEDELJKOVIC, M.; BONYÁR, A. Controlled modification of the surface morphology and roughness of stainless steel 316 by high speed submerged cavitating water jet; **Applied Surface Science**, 458, 2018, pp. 293-304.

[6] ZHAO, J.; JIANG, Z. Thermomechanical processing of advanced high strength steels**; Progress in Materials Science**, 94, 2018, pp. 174-242.

[7] MARTELO, D. F.; MATEO, A. M.; CHAPETTI, M. D.; Fatigue crack growth of a metastable austenitic stainless steel; **International Journal of Fatigue**, 80, 2015, pp. 406-416.

[8] NISHIYAMA, Z. **Martensitic Transformation.** New York: Academic Press, 1978.

[9] ONUKI, Y.; SATO, S. In situ observation for deformation-induced martensite transformation during tensile deformation of SUS 304 stainless steel by using neutron diffraction part II: transformation and texture formation mechanisms. **Quantum beam science**, 5, 6, 2021.

[10] PINEAU, A. G.; PELLOUX, R. M. Influence of strain-induced martensitic transformation on fatigue crack growth rates in stainless steels; **Metall Matter Trans B**, 5, 1974, pp. 1103-1112.

[11] MARTELO, D.F.; MATEO, A.; CHAPETTI, M.D. Crack closure and fatigue crack growth near threshold of a metastable austenitic stainless steels; **Metall. Trans. A**, 21, 1990.

[12] MEI, Z.; MORRIs, J. W. Influence of deformation-induced martensite on fatigue crack propagation in 304-type steels. **Metall. Mater Trans. A**, 21, 1990, pp. 3137-3152.

[13] JAMBOR, M.; VOJTEK, T.; POKORNÝ, P.; SMÍD, M. Effect of solution annealing on fatigue crack propagation in the AISI 304L TRIP steel**. Materials**, 14, 1331, 2021.

[14] LI, Y.; LUO, Y.; LI, J.; SONG, D.; XU, B.; CHEN, X. Ferrite formation and its effect on deformation mechanism of wire arc aditive manufactured 308L stainless steel. **Journal of Nuclear Materials**, 550, 3115, 2021.

[15] LALL, A.; BOWEn, P.; RABIEI, A. Effect of aging on failure mechanism of alloy 709 at various temperatures. **Materials Characterization**, 171, 1044, 2021.

[16] ALSMADI, Z. Y.; ALOMARI, A.; KUMAR, N.; MURTY, K. L. Effect of hold time on high temperature creep-fatigue behavior of Fe-25Ni-20Cr (wt.%) austenitic stainless steel (alloy 709**). Materials Science & Engineering A**, 771, 921, 2020.

[17] ASTM; **Standard test method for strain-controlled fatigue testing**, [S.I], 2-5, p.10, 52. 2012.

[18] LIU, Y.; YANG, y.; MAi, S.; WANG.; SONG, C. Investigation into spatter behavior during seletive laser melting of AISI 316L stainless steel powder. **Materials and Design**, 87, 2015, pp. 797-806.

[19] CARLTON, H. D.; HABOUB, A.; GALLEGOS, G. F.; PARKINSIN, D. Y.; Macdowell, A. A. Damage Evolution and failure mechanisms in additively manufactured stainless steel. **Materials Science & Engineering A,** 651, 2016, pp.406-414.

[20] ZHONG, Y.; RÄNNAR, L.; LIU, L.; KOPTYUG, A.; WIKMAN, S.; OLSEN, J.; CUI, D.; SHEN, Z. Additive manufacturing of 316L stainless steel by eléctron beam melting for nuclear fusion applications. **Journal of Nuclear Materials,,** 486, 2017, pp.234-245.

[21] ZHAO, Y.; LEE, D.; SEOK, M.; LEE, J.; PHANIRAJ, M. P.; SUH, J.; HA, H.; KIM, J.; RAMAMURTY, U.; JANG, J. Resistance of CoCrFeMnNi high-entropy alloy to gaseous hydrogen embrittlement. **Scripta Materialia**, 135, 2017, pp. 54-58.

[22] ORTWEIN, R.; RYS, M.; SKOCZEN, B. Damage Evolution in a stainless steel bar undergoing phase transformation under torsion at cryogenic temperatures. **International Journal of Damage Mechanics**, 25, 2016.

[23] SUN, Q.; JIANG, F.; DENG, L.; XIAO, H.; LI, L.; LIANG, M.; PENG, T.; Uniaxial fatigue behaviour of Cu-Nb micro-composite conductor, part I: Effect of peak stress and stress ratio. **International Journal of Fatigue**, 91, 2016**,** pp. 275-285.
[24] TRÁVNÍCEK, L.; KUBENA, I.; MAZÁNOVÁ, V.; VOJTEK, T.; POLÁK, J.; HUTAR, P.; SMÍD, M. Advantageous description of short fatigue crack growth rates in austenitic stainless steels with distinct properties. **Metals**, 11, 475, 2021.